CI&CEQ
Chemical Industry & Chemical Engineering Quarterly

Available online at
Association of the Chemical Engineers of Serbia AChE
www.ache.org.rs/CICEQ

Chem. Ind. Chem. Eng. Q. 29 (3) 243–252 (2023) CI&CEQ

ALANNA SILVEIRA DE MORAES[1]
GABRIELA OLIVEIRA CASTRO PONCINELLI[1]
ARON SEIXAS TERRA RODRIGUES[1]
LAISE FAZOL DO COUTO[1]
SILVIA LUCIANA FÁVARO[2]
RITA DE CÁSSIA COLMAN [1]

[1]Universidade Federal Fluminense, Chemical Engineering and Petroleum Department, RJ, Brazil

[2]Universidade Estadual de Maringá – Mechanical Engineering Department, Maringá, PR, Brazil

SCIENTIFIC PAPER

UDC 544.47:66:547

STUDY OF CATALYTIC OXIDATION OF TOLUENE USING Cu-Mn, Co-Mn, AND Ni-Mn MIXED OXIDES CATALYSTS

Article Highlights

- Nanocrystalline AMn2O4 (A = Co, Ni, Cu) spinel-type mixed oxides were tested for VOC removal
- Spinel oxides are important due to their high thermal resistance, selectivity, and electronic properties
- The higher activity of NiMn oxide than CoMn and CuMn is due to a higher Mn^{3+} content
- The activity is also attributed to the synergistic effect of manganese on spinel and Ni^{2+} cations

Abstract

The successful synthesis of AMn_2O_4 (A = Co, Cu, and Ni) spinels via solution combustion was achieved in less time than other methods. All catalysts with the same fuel/nitrate ratio were used to oxidize toluene, and the relationship between their properties and activities was investigated. Among all, nickel manganite exhibited the most promising activity, and by changing the fuel/nitrate ratio, it was sought to obtain the most appropriate structure for the reaction studied. Physico-chemical analysis was used to define the characteristics of the synthesized catalysts. The results showed the successful synthesis of spinels and indicated that other materials peaks (single oxide phases) exist in the catalyst structure. BET-BJH analyses reveal the mesoporous structures and, given the limitations of the equipment, were all classified as less than 10 m^2/g. The SEM images evidence the influence of the urea content used. The particle size increases at higher fuel/nitrate ratios. Samples of NiMn1.67 and NiMn2.08 showed larger and denser, sparsely dispersed clusters. Simultaneously considering reactor analysis and test results, it was found that the synthesized catalyst with a fuel/nitrate ratio of 0.5 has the best performance on toluene oxidation.

*Keywords: **s**olution combustion synthesis, fuel-to-nitrates ratio, manganite spinels, toluene oxidation.*

Due to concerns of medical and scientific communities about the increase of volatile organic compounds (VOCs) in the atmosphere and the cost of reducing anthropogenic emissions, the development of appropriate forms of disposal or transformation has received a lot of attention. [1,2].

The U.S. Environmental Protection Agency (EPA) describes VOCs as a relevant group of many carbon compounds, excluding monoxide carbon, carbon dioxide carbon, acid carbon, metallic carbide or carbonate, and ammonium carbonate, which presents high atmospheric photochemical activities. VOCs are harmful to human health and the environment because of their toxicity, and they are a precursor of smog photochemical and ozone formation in the atmosphere [3,4]. Thus, the need to control and treat air pollution has become urgent. It is clearly evident in the numerous global, national, and regional environmental pollution control regulations developed to maintain healthy air

Correspondence: R. De Cássia Colman, Universidade Federal Fluminense, Chemical Engineering and Petroleum Department, Passo da Pátria Street, 156/bl E/102-A, CEP: 24210-240, Niterói, RJ, Brazil.
E-mail: ritacolman@id.uff.br
Paper received: 19 April, 2022
Paper revised: 22 August, 2022
Paper accepted: 14 December, 2022

https://doi.org/10.2298/CICEQ220419031M

quality. These strict standards have led the industrial and commercial sectors to rely on carbon adsorption, incineration, or purification technologies to reduce the environmental damage caused by technological advances [5,6].

Different techniques for controlling VOC emissions are divided into process and equipment modification and treatment techniques. The first one, also known as indirect measures, is characterized by the changes in the process, the raw material change, and equipment maintenance. The second group of direct measurements is characterized by destruction techniques (oxidation and biofiltration, for example) and recovery (such as membrane separation, absorption, adsorption, and condensation) [7,8].

In this context, catalytic oxidation is an interesting technology because it eliminates or transforms VOCs at relatively low temperatures (200 °C–450 °C), minimizes the formation of by-products, such as NOx, and can be effectively applied over a wide range of VOC concentrations (up to 10,000 ppm) and highly recommended when highly diluted (about 1,000 ppm) [9–11]. Moreover, from an economic point of view, catalytic oxidation is also an attractive alternative due to the low energy consumption and lower cost of by-product treatments that are not practically formed [12,13].

Mixed transition metal oxides exhibit greater activities and stabilities than simple oxides because these metals can have more than one valence state, a property determined by the electronic configuration of the metal d level [14,16]. Compared to supported noble metal catalysts, mixed oxides have lower costs and higher resistance to impurities. Among the oxides of the present invention, the spinel-like structure has also been highlighted due to its high thermal resistance, selectivity, and electronic properties, which improve oxide reducibility [17–19].

The synthesis by solution combustion (SCS), also known as self-combustion or self-propagating, has gained prominence since it combines the advantages of the sol-gel technique with a good stoichiometry control, making it possible to synthesize homogeneous oxides and high purity [20–21]. In addition, the method combines good textural properties and excellent dispersion and distribution of the active phase obtained in short synthetic times compared to other methods [22]. This method involves the autoignition of an aqueous solution containing oxidizing reagents, such as nitrates, sulfates, and metal carbonates, and reducing reagents (also called fuels), such as urea, citric acid, and glycine. The heat required to conduct the reaction is provided by the process and not from an external source. It is due to the exothermic and self-catalytic reactions that occur when the reactants reach the ignition temperature. The formation of a large amount of gases is a characteristic of the reactions. For example, 1 mol of the synthesized catalyst generates 22 moles of gases. The powder obtained after cessation of combustion may be a single phase or a combination of various metal oxides [22,24].

The characteristics of the powders synthesized by the SCS are mainly governed by the temperature reached when combustion occurs effectively. In turn, it depends exclusively on the type and amount of fuel used, so the fuel/nitrate ratio is considered one of the important parameters. In a more detailed study, careful analysis can be made of its influence on synthesized materials' phase formation and crystallite size.

The present work aims to obtain by SCS the mixed oxides type AMn_2O_4 (A = Co, Cu, and Ni), to evaluate its catalytic activities on toluene oxidation, and to evaluate the effect of different fuel/nitrate ratios on the physicochemical characteristics and catalytic activity of the $NiMn_2O_4$ catalyst.

EXPERIMENTAL

Catalysts preparation

For the synthesis of catalysts using the solution combustion method, the following nitrates (Sigma Aldrich®, 99.999%): $Mn(NO_3)_2{\cdot}4H_2O$, $Co(NO_3)_2.6H_2O$, $Cu(NO_3)_2.6H_2O$, and $Ni(NO_3)_3{\cdot}6H_2O$, and urea (NH_2CONH_2; Quimibrás, 99.5%) were used without any purification. The steps of combustion synthesis of catalysts are shown in Supplementary Information.

The reagents (nitrates and urea) were dissolved in 20 mL of deionized water and placed in a porcelain beaker. The solution obtained was placed under constant heating and stirring, and as the temperature increased and the water evaporated, the solution became viscous. The color of the solution also changed with increasing temperature, becoming progressively darker until it became completely black (Supplementary Information).

Near the ignition point, the solution's temperature drops rapidly away from the set point. However, combustion occurred, and the gaseous products were released as yellow smoke, forming a fine black powder (catalyst). The material obtained was weighed and calcined at 700 °C for 6 h to ensure spinel phase formation and to eliminate any presence of carbonaceous residues.

The abbreviated names were chosen to name the synthesized catalysts: Mn_3O_4, CoMn0.5, CuMn0.5, NiMn0.5, NiMn1.25, NiMn1.67, and NiMn2.08. In this nomenclature system, AMn (A=Co, Cu, or Ni) stands for AMn_2O_4, and the number indicates the fuel-to-

nitrates fuel/nitrate ratios of 0.5, 1.25, 1.67, or 2.08.

Catalysts characterization

The textural properties of the catalysts were determined using N_2 isotherms measured at −196 °C by a Micromeritics® ASAP 2420 instrument. The specific surface area (S_{BET}) was determined by the Brunauer-Emmett-Teller (BET) [25], and the pore volume and pore size distribution were calculated by the Barret-Joyner-Halenda (BJH) method [26].

The composition of the phases present in the samples was determined by the XRD technique in a Rigaku® Miniflex diffractometer using CuKα radiation (λ = 1.54056 Å). Diffraction patterns were collected over the 2θ range of 15°–70° with a step size of 0.02°. From the obtained diffractograms, it was possible to determine the crystalline phases present by comparison with peaks of known and tabulated materials and the average size of the lens of the metallic species by the Scherrer equation.

Fourier-transform infrared (FTIR) spectra were recorded on a Perkin Elmer spectrometer (System 2000). The samples were pressed into self-supported wafers and placed into a glass cell sealed by KBr windows in 3% (w/w) proportions; 32 successive scans were performed for each spectrum obtained.

The morphology of the oxides was analyzed by scanning electron microscopy using a high vacuum mode DEI QUANTA 250 apparatus with a voltage of 30 kV.

The analysis of temperature-programmed reduction with H_2 (TPR) was conducted with a Micromeritics® AutoChem 2920 under atmospheric pressure. Catalyst samples (0.3 g) were subjected to reduction using 10 vol.% H_2 in N_2 at 30 cm^3/min and a linear heating rate of 10 °C/min from room temperature to 1000 °C.

Evaluation of catalytic performance

The samples were evaluated for catalytic oxidation of toluene. The reactions were carried out at atmospheric pressure in a continuous fixed bed U- shaped tubular reactor. The total flow rate of the reactant mixture (20% O_2 in He + 1000 ppm toluene) was 150 ml/min. The catalyst (0.1 g) was mixed with silicon carbide (SiC, 0.4 g) to avoid the effect of hot spots and deposited on a quartz wool plug. A tied thermocouple continuously monitored the temperature. First, the catalysts were reduced in an H_2 stream at their respective reduction temperature for 1 h. Then, the catalysts were evaluated at 100 °C, 200 °C, 300 °C, and 400 °C, under a mixture of O_2, toluene, and He (20% O_2, 1000 ppm toluene, and He to complete the balance), with a total flow of 150 mL/min After remaining at each test temperature for 24 hours, the catalysts were heated under a helium flow to the next test temperature. In this way, it was also possible to evaluate the stability of the catalyst.

The products and reagents were analyzed by gas chromatography (Agilent® 7890A) equipped with a thermal conductive detector (TCD) and a flame ionization detector (FID) using a Porapak N column.

The products and reagents were analyzed by an Agilent® 7890A gas chromatograph with a flame ionization detector (FID) and thermal conductivity detector (TCD). The conversion of toluene (X%) was calculated according to Eq. (1):

$$X\% = \frac{[Tol]_{in} - [Tol]_{out}}{[Tol]_{in}} \times 100 \quad (1)$$

where $[Tol]_{in}$ and $[Tol]_{out}$ denote the inlet and outlet concentrations of toluene, respectively.

RESULTS AND DISCUSSION

According to the results obtained for N_2 adsorption (Figure 1), the isotherms used for all samples are classified in category type IV (of the IUPAC classification) and reveal the adsorption characteristics in multilayer related to weak interactions in mesoporous-containing materials (pore diameter between 2 and 50 nm). Isotherms of this type have defined levels and indicate capillary condensation [27].

It is also observed that the desorption curve does not coincide with the adsorption curve, a phenomenon known as hysteresis, due to the saturation pressure of N_2 being different in the condensation and evaporation from inside the pores. In all isotherms, the present hysteresis is of type H1, characterized by two branches of almost parallel isotherms. This hysteresis loop was observed at high relative pressures (P/Po ≈ 0.7 to 0.9) and is generally associated with materials of mesoporous structures and a representative of an adsorbent consisting of rigid agglomerates of spherical particles and relatively uniform pore distribution [28,29].

It is also observed that the practically parallel branches of the adsorption and desorption isotherms of the CuMn0.5 sample are more vertical when compared to the other isotherms, indicating that the mesoporous size distribution is narrower. The lower values of relative pressure in the capillary condensation (around 0.2) in the Mn0.5 catalyst isotherm compared to the other synthesized catalysts, with a fuel/nitrate ratio of 0.5 to about 0.4, indicate a decrease in mesoporous size [27].

Although all surface areas were classified as less than 10, due to the limitation of the equipment used, the

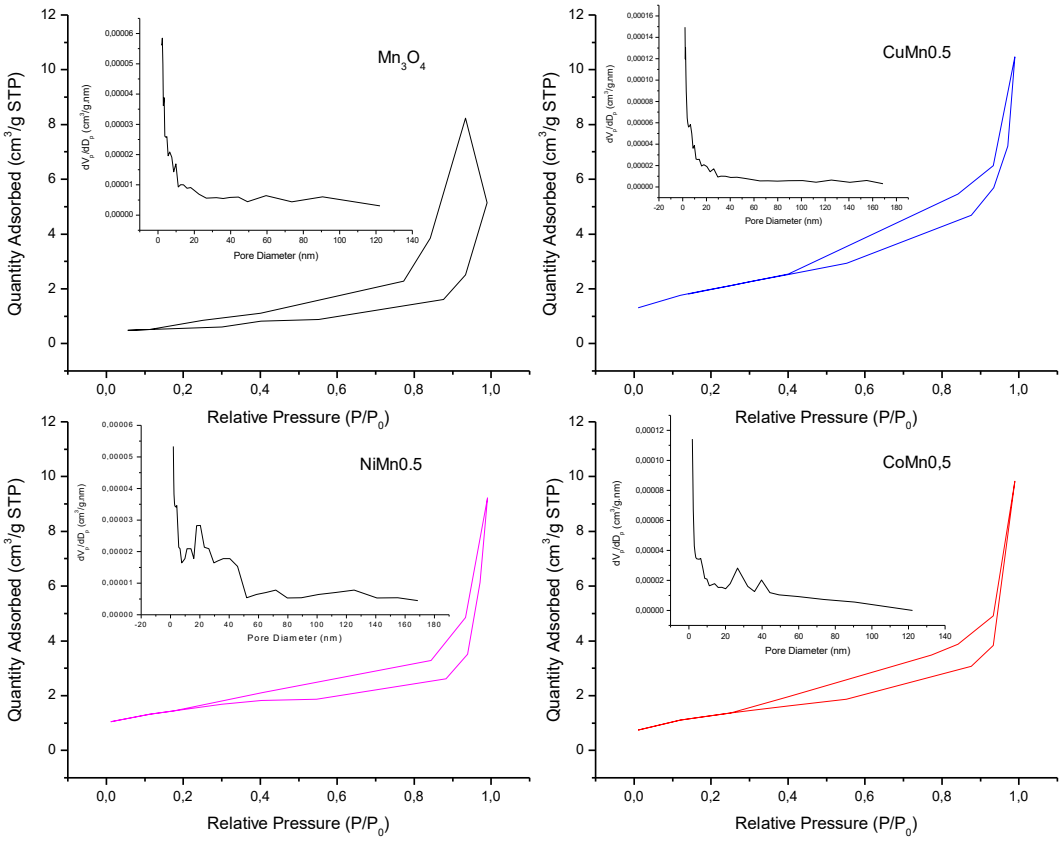

Figure 1. Adsorption/Desorption isotherms and BJH pore size distribution of the catalysts with a fuel/nitrate ratio of 0.5.

average pore diameter obtained by BJH was above 2 nm for all samples, the NiMn0.5 catalyst being with the largest distribution of mesoporous diameter (between 2 nm and 50 nm). Therefore, the surface area (S_{MESO}) and the volume (V_{MESO}) of the mesoporous are listed in Table 1.

The synthesized catalysts with different fuel/nitrate ratios, such as NiMn1.25 and NiMn1.67, present type IV isotherms indicating mesoporous formation (Supplementary Information). It can also be observed that there is a region (P/P ≈ 0.85) where the adsorbed volume increases sharply while the relative pressure varies little. The present hysteresis of the isotherms is of type H1 with two branches of parallel isotherms, indicating complete mesoporous filling at a relative pressure of less than 1. This hysteresis also represents an adsorbent with a narrow distribution of relatively uniform pores [27].

The isotherm of the NiMn2.08 sample is of type V, characteristic of low adsorbent-adsorbate interaction. However, there is pore filling and hysteresis type H2. This hysteresis also characterizes mesoporous structure materials but is associated with a more complex structure with poorly defined pore size and shape distribution [28,29].

Table 1. The textural properties of the catalysts.

Catalyst	S_{MESO} (m²/g)	V_{MESO} (cm³/g)
Mn0.5	1.28	0.0018
CoMn0.5	3.82	0.0142
CuMn0.5	5.68	0.0159
NiMn0.5	4.32	0.0143
NiMn1.25	0.94	0.0012
NiMn1.67	0.71	0.0008
NiMn2.08	0.02	0.0004

The data obtained from the adsorption/desorption analysis of N_2 allowed one to determine the surface areas of the samples. Still, given the limitations of the equipment, they were all classified as less than 10 m^2/g. The average pore diameter obtained by BJH is greater than 2 nm for all samples; the sample with a fuel rate of 0.5 has the largest pore distribution diameter (between 2 and 50 nm). These specifications are probably due to

the implementation of the proper fuel/nitrate ratio resulting in necessary and sufficient heat generation for combustion. Consequently, the proper gas volume was created during combustion. It is also possible to observe that the synthesized catalysts with a fuel/nitrate ratio of 1.25 and 1.67 have a very similar pore distribution diameter (between 2 nm and 40 nm), probably due to sufficient fuel availability during the synthesis process. But with a further increasing fuel/nitrate ratio to 2.08, larger crystals were formed due to increasing burning heat, reducing pore distribution diameter (between 2 nm and 30 nm).

Figure 2a presents the XRD results for the synthesized catalysts with a fuel/nitrate ratio equal to 0.5.

Through a comparative study between crystallographic reference chips of pure materials and the diffractograms obtained, it was possible to identify the diffraction lines characteristic of the structure Mn_3O_4 (♦) with basic orthorhombic geometric structure in all samples, being more present in CoMn0.5. Furthermore, the CoMn0.5 sample also shows characteristics of $MnCo_2O_4$ (*), cubic and face-centered spinel.

The CuMn0.5 catalyst showed little similarity with the characteristic peaks of the less intense Mn_3O_4 structure, suggesting a loss of crystallinity. In addition, peaks related to the $CuMn_2O_4$ spinel structure (°), with cubic and face-centered structure, were also identified.

In the diffractogram of the NiMn0.5 sample, the characteristic $NiMn_2O_4$ spinel peaks (•) and cubic face-centered structure. The $NiMnO_3$ and NiO secondary phases, with diffraction peaks coinciding with those of the main phase, were possibly identified.

Figure 2b shows the X-ray diffraction (XRD) results for $NiMn_2O_4$ prepared by the combustion method with four different fuel/nitrate ratios. The formation of a spinel structure and some impurities of metal oxide (NiO and Mn_3O_4) were confirmed in all catalysts. In addition, the peaks in 2θ = 23.1, 32.9, 55.1, and 65.9 were ascribed to the presence of Mn_3O_4 (PCPDFWIN 750765).

The diffraction lines corresponding to the Mn_3O_4 (♦) structure were observed in all samples. In addition, the peaks related to $NiMn_2O_4$ (●), 2θ = 23.9, 34.1, 36.9, 41.7, 50.2, and 64.0 (PCPDFWIN 011110), cubic face-centered structure, and possibly $NiMnO_3$, 2θ = 35.7, 39.3, and 49.1 (PCPDFWIN 120269), and NiO, 2θ = 37.2, 43.2, and 62.9 (PCPDFWIN 780643); secondary phases were also identified. The intensity of these peaks generated in most $NiMn_2O_4$ phases was inversely proportional to the fuel/nitrate ratio; the increased fuel amount used decreased the catalyst crystallinity. The average crystallite size calculated based on the peak around 36° for the NiMn1.25, NiMn1.67, and NiMn2.08 catalysts were 21, 18.2, and 16.7 nm, respectively.

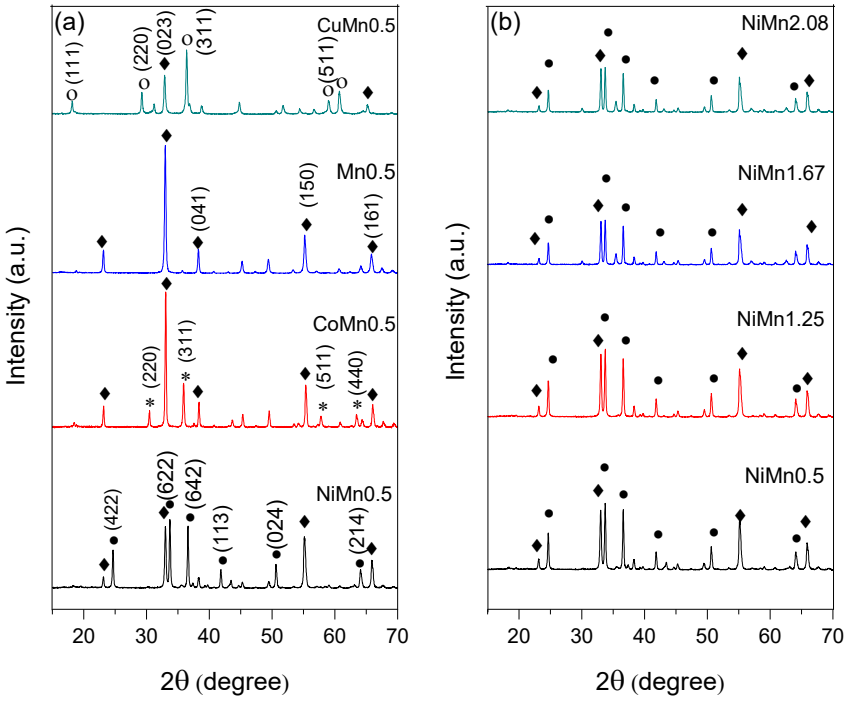

Figure 2. XRD patterns of (a) the catalysts with a fuel/nitrate ratio of 0.5 and (b) the $NiMn_2O_4$ catalysts with various fuel ratios.

FTIR analysis of the synthesized samples with a fuel/nitrate ratio of 0.5 was done in the 500 cm^{-1}–4000 cm^{-1} wavelength range and shown in Figure 3a. The urea peak was not detected in any sample, generally indicated by a peak around 1700 cm^{-1}, due to the stretching of the double bond between C atoms. In this case, it was assumed that all the fuel was consumed in synthesizing the catalysts with a fuel/nitrate ratio of 0.5 [30,31]. The vibration peak of NO_3 groups appearing at 900 cm^{-1}, 1360 cm^{-1}, and 1560 cm^{-1} was also not detected, indicating a total consumption of nitrate compounds in the samples [32,33]. Strong peaks formed at 400 cm^{-1}–700 cm^{-1} may be related to the formation of spinel structure [12;34].

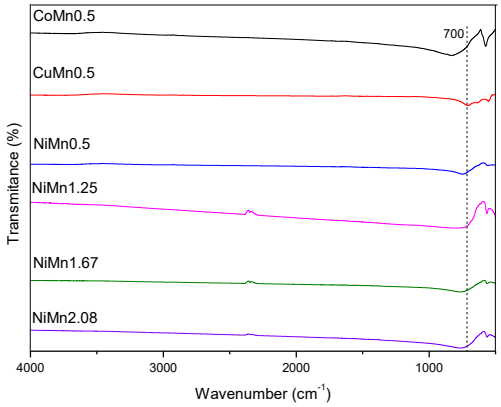

Figure 3. FTIR spectra of the catalysts with a fuel/nitrate ratio of 0.5 and the $NiMn_2O_4$ catalysts with various fuel/nitrate ratios.

The spinel structure in these samples was confirmed by the FTIR results (Figure 3b). According to the FTIR spectrum of the Ni catalysts with various fuel/nitrate ratios, the formation of the spinel structure in all mixed oxides can be confirmed. The bands formed below 1000 cm^{-1} are attributed to the metal-oxygen bonds (MOM), and in the range between 700 cm^{-1} and 400 cm^{-1} are characteristics of the AB_2O_4 structure [34]. The band near 700 cm^{-1} is attributed to the stretching vibrations of the Mn-O group coordinated in a tetrahedron. The vibrations corresponding to the stretching of the M-O group of octahedral coordination are observed around 517 in all catalysts [12,34].

As the urea content in the synthesis of the Ni and Mn catalysts increases, the intensity of the vibrations, characteristic of the spinel structure (between 700 and 400 cm^{-1}), decreases. It can be explained by the dependence of the band intensity on the number of responsible bonds; that is, the oxides obtained with the lowest fuel/nitrate ratios show more bands attributed as spinel structures [35].

The H_2-TPR experiments of synthesized catalysts with a fuel/nitrate ratio of 0.5 and the maximum consumption temperatures are shown in Figure 4a. The Mn_3O_4 sample has two peaks, one starting at approximately 270 °C and another between 400 °C and 510 °C. According to the literature, the first one possibly refers to the reduction of Mn_2O_3 to Mn_3O_4 ($Mn^{3+} \rightarrow Mn^{3+}/Mn^{2+}$), and the second to the reduction of Mn_3O_4 to MnO ($Mn^{3+}/Mn^{2+} \rightarrow Mn^{2+}$) [36].

The sample reduced at lower temperatures is CoMn0.5, with two reduction peaks. The first one is between 100 °C and 250 °C, corresponding to the reduction of Co_3O_4 to Co^0 ($Co^{2+}/Co^{3+} \rightarrow Co^{2+} \rightarrow Co^0$), and the second one between 300 °C and 450 °C, related to the reduction of $CoMn_2O_4$ ($Co^{2+} \rightarrow Co^0$) [12]. The CuMn0.5 catalyst showed only a reduction peak between 200 °C and 400 °C, related to the $CuMn_2O_4$ reduction ($Cu^{2+}/Cu^{1+} \rightarrow Cu^0$) [12].

The NiMn0.5 catalyst showed the highest peaks near the peak range presented by the Mn0.5 sample. For example, a peak between 250 °C and 430 °C refers to the reduction of $NiMn_2O_4$ and $NiMnO_3$ to NiO ($Ni^{3+} \rightarrow Ni^{2+}$), and another between 400 °C and 600 °C refers to the reduction of NiO to Ni^0 [23].

The H_2-TPR experiments of $NiMn_2O_4$ synthesized with a different fuel/nitrate ratio and the maximum consumption temperatures are shown in Figure 4b. It can be observed that all NiMn samples showed similarities in the reduction profiles, with two characteristic peaks attributed to the decomposition of surface species $NiMn_2O_4$ and $NiMnO_3$/NiO → MnO/Ni → MnO. The NiMn1.25 catalyst has the peak of the first major reduction, indicating the presence of more $NiMn_2O_4$ structures [23]. For this catalyst, a shift of the peaks towards the lowest temperature is observed. In the case of NiMn1.67 and NiMn2.08, a possible stronger interaction between manganese and nickel made the reduction more difficult. This effect can also be attributed to the increased partial water pressure in the catalyst pores as the particle diameter increases [22].

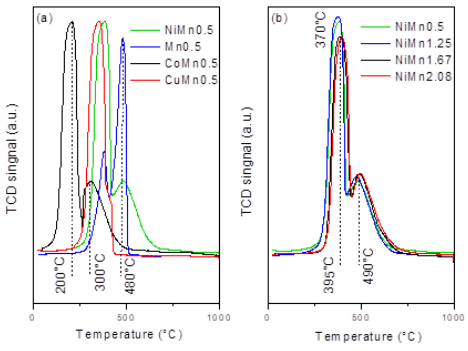

Figure 4. TPR curves for (a) the catalysts with a fuel/nitrate ratio of 0.5 and (b) the $NiMn_2O_4$ catalysts with various fuel ratios.

Figure 5 shows the surface morphology of the samples with the same fuel/nitrate ratio (0.5). From the analysis of micrographs, we can observe the formation of aggregate particles in the form of grains, which tend to aggregate and grow due to the high temperatures reached during the synthesis. The addition of a second metal made these grains smaller.

Among the synthesized oxides with a fuel/nitrate ratio of 0.5, the CoMn0.5 was with the largest agglomerates, and the NiMn0.5 was with the smallest ones. The surfaces of the CoMn0.5 and Mn_3O_4 samples have voids in their structure, attributed to the evolution of larger quantities of gases during combustion [37].

The morphology and the particle size distribution of the Ni catalysts with various fuel/nitrate ratios (Supplementary Information) also indicated that the influence of the urea content used is evidenced by observing that the structure of the obtained powders changes with increasing particles as the fuel/nitrate ratio is increased. It is also observed that the NiMn0.5 and NiMn1.25 samples have the most homogeneous surface, while the NiMn1.67 and NiMn2.08 samples have bigger and denser, occasionally dispersed clusters.

Figure 6 shows the catalytic performances of the catalysts in toluene combustion. The evaluation of the catalytic performance of all catalysts synthesized with a fuel/nitrate ratio equal to 0.5 showed conversion of 100% of toluene at 300 °C, while this conversion to Mn_3O_4 was only observed at 400 °C; this increase in catalytic activity is attributed to the addition of the second metal (Co, Cu, and Ni).

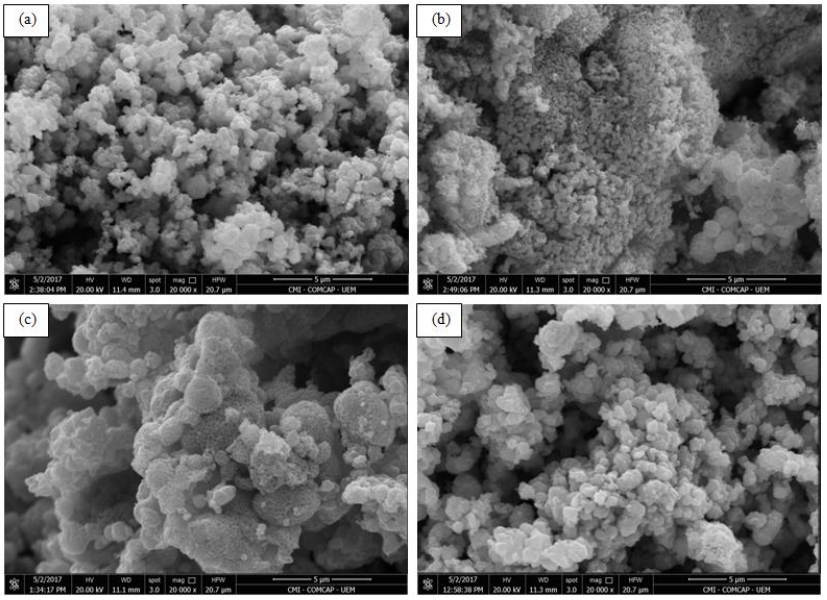

Figure 5. SEM images of the catalysts with a fuel/nitrate ratio of 0.5: (a) CoMn0.5, (b) CuMn0.5, (c) NiMn0.5, and (d) Mn_3O_4.

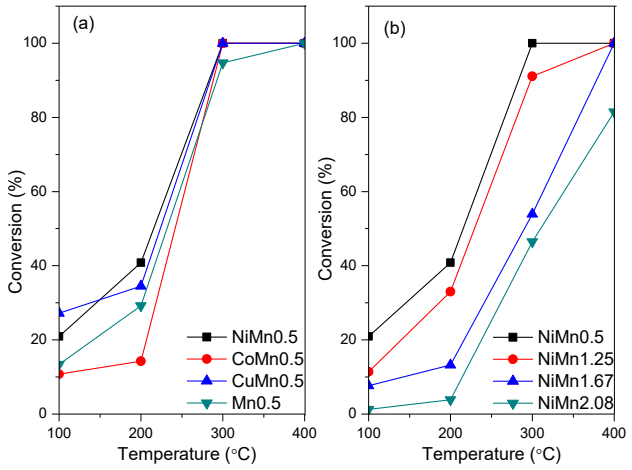

Figure 6. Curves for converting toluene over (a) the catalysts with a fuel/nitrate ratio of 0.5 and (b) the $NiMn_2O_4$ catalysts with various fuel ratios.

At the lowest temperature (100 °C), the catalyst CuMn0.5 showed the best conversion (27%), but NiMn0.5 was more active for toluene oxidation at higher temperatures. Although the synergistic interactions between Mn^{3+} and Ni^{2+} cations by oxygen bonds increase the catalytic activity at higher temperatures (>200 °C), the increase of the Ni^{2+} ions in the synthesized powders improves the reducibility of mixed oxides.

CoMn0.5 was less active at temperatures below 300 °C. This performance, combined with the XRD, FTIR, and TPR results, may indicate that CoMn0.5 presents a lower number of active Mn^{3+} and Co^{2+} sites than the other synthesized samples with a fuel/nitrate ratio of 0.5. Likewise, the highest activity of the NiMn oxide is attributed to the high content of Mn^{3+} and the synergistic effect between manganese in the spinel and Ni^{2+} cations.

NiMn0.5 showed the highest activity than others. It can be observed that the synergistic effect, together with the smaller synthesized NiMn catalysts, showed better catalytic activity (NiMn0.5> NiMn1.25> NiMn1.67> NiMn2.08). Only the NiMn0.5 catalyst converted 100% toluene at 300 °C, while the maximum conversion obtained with NiMn2.08 was 81% at 400 °C.

Upon analyzing the results of the catalytic tests and the analysis of XRD, TPR, and FTIR, higher activities for the NiMn2O4 and CuMn2O4 catalysts can be observed compared to the $CoMn_2O_4$ catalyst. It can be attributed to the presence of active sites of Mn^{3+}, $Ni^{2+,}$ and Cu^{2+}. Likewise, the largest activity of $NiMn_2O_4$ is attributed to the highest content of Mn^{3+} and the synergistic effect of manganese on spinel and Ni^{2+} cations [38]. The catalytic performance of NiMn0.5 for toluene oxidation was compared with the literature that reported mixed oxides and noble metal catalysts, as shown in Table 2.

Table 2. Comparison of the catalytic performance between NiMn0.5 and other literature reported catalysts.

Catalyst	Catalyst mass (g)	Toluene concentration (ppmV)	T_{90}[a] (°C)	Ref.
Co_2AlO_x	0.4	530	284	[39]
5%Co/Al_2O_3	0.2	1000	368	[40]
5%Cu/Al_2O_3			363	
Cu_4FeO_x	0.1	800	294	[41]
Au/CeO_2–Al_2O_3			280	
Ag/CeO_2–Al_2O_3			350	
Pd/CeO_2–Al_2O_3	0.05	1000	220 190	[42]
Pt/CeO_2–Al_2O_3				
NiMn0.5	0.1	1000	282	This work

[a]T_{90} is the temperature at the time of conversion of 90% toluene.

VOC oxidation occurs according to a Mars-van Krevelen-type redox cycle, which involves the adsorption of VOC and its subsequent oxidation by lattice oxygen and adsorbed oxygen atoms [43]. Since the mechanism involves the exchange of oxygen between the lattice and gas phase and oxidation of CO, oxygen mobility in the redox cycle and the surface acidity for breaking carbon-carbon bonds are important in hydrocarbon oxidation [44]. Although the correlation of acidity with the activity in oxidation reactions is still a subject of debate, it can be stated that the acid-base properties of mixed oxides may have a key role in controlling the kinetics of adsorption-desorption of the reactants and intermediate species [45]. In this case, metallic couples must be in different oxidation states for the reaction to occur. The more active sites, the greater the activity of the catalysts for the reaction. If more active Mn^{3+} and Ni^{2+} sites are present in the $NiMn_2O_4$ sample, this will justify its higher catalytic activity [12,38].

CONCLUSION

The spinel structure in all catalysts has gained prominence due to its high thermal resistance, selectivity, and electronic properties, which improve oxide reducibility.

The higher activity of NiMn oxide is attributed to the higher Mn^{3+} content and the synergistic effect of manganese on spinel and Ni^{2+} cations. This effect, added to the larger areas of the synthesized NiMn catalysts with lower fuel/nitrate ratios, gives the lower urea catalysts better catalytic activity. The synergistic effect added to the larger areas of smaller synthesized NiMn catalysts gave the lowest urea catalyst the best catalytic activity (NiMn0.5> NiMn1.25> NiMn1.67> NiMn2.08). Furthermore, the catalyst toluene conversion temperature of 100% studied in the present work is compatible with commercially used Au-based catalysts, which are more expensive and susceptible to poisoning.

ACKNOWLEDGEMENTS

This study was financed in part by the Coordenação de Aperfeiçoamento de Pessoal de Nível Superior – Brasil (CAPES) – Finance Code 001. The authors also gratefully acknowledge Federal Fluminense University for complementary support.

REFERENCES

[1] L. Pei, W. Yin, J. Wang, J. Chen, C. Fan, Q. Zhang, Mater. Res. 13 (2010) 339–343. https://doi.org/10.1590/S1516-14392010000030001.

[2] C. He, J. Cheng, X. Zhang, M. Douthwaite, Z. Hao, Chem.

Rev. 119 (2019) 4471–4568. https://doi.org/10.1021/acs.chemrev.8b00408.
[3] S. Hosseini, Adv. Ceram. Sci. Eng. 5 (2016) 1–10. https://doi.org/10.14355/acse.2016.05.001.
[4] R. Fang, J. Huang, X. Huang, X. Luo, Y. Sun, F. Dong, H. Huang, Chemosphere 289 (2022) 2–10. https://doi.org/10.1016/j.chemosphere.2021.133081.
[5] M. Castaño, R. Molina, S. Moreno, Appl. Catal., A 492 (2015) 48–59. https://doi.org/10.1016/j.apcata.2014.12.009.
[6] J. Li, W. Cui, P. Chen, X. Dong, Y. Chu, J. Sheng, Y. Zhang, Z. Wang, F. Dong, Appl. Catal. B Environ. 260 (2020) 118130–118136. https://doi.org/10.1016/j.apcatb.2019.118130.
[7] E. Genty, S. Siffert, R. Cousin, Catal. Today 333 (2019) 28–35. https://doi.org/10.1016/j.cattod.2018.03.018.
[8] A. Kostyniuk, D. Bajec, B. Likozar, J. of Ind. Eng. Chem. 96 (2021) 130–143. http://dx.doi.org/10.1016/j.proci.2006.07.052.
[9] C. Gennequin, S. Siffert, R. Cousin, A. Aboukaïs, Top. Catal. 52 (2009) 482–491. https://doi.org/10.1007/s11244-009-9183-7.
[10] F. Aguero, B. Barbero, L. Gambaro, L. Cadús, Appl. Catal., B 91(2009) 108–112. http://dx.doi.org/10.1016/j.apcatb.2009.05.012.
[11] B. Silva, H. Figueiredo, V. Santos, M. Pereirab, J. Figueiredo, A.Lewandowskac, M. Bañares, I.Neves, T. Tavaresa, J. Hazard. Mater. 192 (2011) 545–553. https://doi.org/10.1016/j.jhazmat.2011.05.056.
[12] S. Hosseini, A. Niaei, D. Salari, S. Nabavi, Ceram. Int. 38 (2012) 1655–1661. https://doi.org/10.1016/j.ceramint.2011.09.057.
[13] B. Langford, Atmos. Chem. Phys. 10 (2010) 8391–8412. https://doi.org/10.5194/acp-10-8391-2010.
[14] C. Bozo, N. Guilhaume, E. Garbowski, M. Primet, Catal. Today 59 (2000) 33–45. https://doi.org/10.1016/S0920-5861(00)00270-4.
[15] N. Kumar, K. Jothimurugesan, G. Stanley, V. Schwartz, J. Spivey, J. Phys. Chem. C 115 (2011) 990–998. https://doi.org/10.1021/jp104878e.
[16] W. Wen, J. Wu, RSC Adv. 4 (2014) 58090–58100. https://doi.org/10.1039/C4RA10145F.
[17] J. Védrine, Met. Oxides Heterog. Catal. , Elsevier B.V. (2018) 551–569. https://doi.org/10.1016/B978-0-12-811631-9.00009-0.
[18] S. Saqer, D. Kondarides, X. Verykios, Appl. Catal., B 103 (2011) 275–286. https://doi.org/10.1016/j.apcatb.2011.01.001.
[19] V. Radonjić, J. Krstić, D. Lončarević, N. Vukelić, D. Jovanović, Chem. Ind. Chem. Eng. Q. 25 (2019) 193–206. https://doi.org/10.2298/CICEQ181001032R.
[20] S. Aruna, A. Mukasyan, Solid State Mater. Sci. 12 (2008) 44–50. https://doi.org/10.1016/j.cossms.2008.12.002.
[21] J. Baneshi, M. Haghighi, N. Jodeiri, M. Abdollahifar, H. Ajamein, Ceram. Int. 40 (2014) 14177–14184. https://doi.org/10.1016/j.ceramint.2014.06.005.
[22] A. Varma, A. Mukasyan, A. Rogachev, K. Manukyan, Chem. Rev. 116 (2016) 14493–14586. https://doi.org/10.1021/acs.chemrev.6b00279.
[23] M. Ouaguenouni, A. Benadda, A. Kiennemann, A. Barama, C. R. Chim. 12 (2009) 740–747. https://doi.org/10.1016/j.crci.2008.12.002.
[24] D. Jeong, W. Jang, J. Shim, H. Roh, Int. J. Hydrogen Energy 41 (2016) 3870–3876. https://doi.org/10.1016/j.ijhydene.2016.01.024.
[25] S. Brunauer, P. Emmett, E. Teller, J. Am. Chem. Soc. 60 (1938) 309–319. https://doi.org/10.1021/ja01269a023.
[26] L. Joyner, E. Barret, , R. Skold, J. Am. Chem. Soc. 73 (1951) 3155–3158. https://doi.org/10.1021/ja01151a046.
[27] T. Horikawa, D. Do, D. Nicholson, Adv. Colloid Interface Sci. 169 (2011) 40–58. https://doi.org/10.1016/j.cis.2011.08.003.
[28] G. Ertl, H. Knözinger, J. Weitkamp, Handb. Heterog. Catal. (2nd Ed.) , Germany: VCH Verlagsgesellschaft mdH, (1997), 49–138. https://doi.org/10.1002/9783527619474.
[29] K. Sing, Pure & Appl. Chem. 57 (1985) 603–619. https://doi.org/10.1351/pac198557040603.
[30] L. Bach, B. Quynh, V. Thuan, C. Thang, K. Lim, J. Nanosci. Nanotechnol. 16 (2016) 8482–8485. https://doi.org/10.1166/jnn.2016.12511.
[31] A. Saberi, F. Golestani-Fard, H. Sarpoolaky, M. Willert-Porada, T. Gerdes, R. Simon, J. Alloys Compd. 462 (2008) 142–146. https://doi.org/10.1016/j.jallcom.2007.07.101.
[32] Y. Huang, Y. Tang, J. Wang, Q. Chen, Mater. Chem. Phys. 97 (2006) 394–397. https://doi.org/10.1016/j.matchemphys.2005.08.035.
[33] M. Taibi, S. Ammar, N. Jouini, F. Fievet, P. Molinie, M. Drillon, J. Mater. Chem. 12 (2002) 3238–3244. https://doi.org/10.1039/B204087E.
[34] A. Salker, S. Gurav, J. Mater. Sci. 35 (2000) 4713–4719. https://doi.org/10.1023/A:1004803123577.
[35] R. Zampiva, C. Junior, A. Alves, C. Bergmann, FME Transactions. 46 (2018) 157–164. https://doi.org/10.5937/fmet1802157Z.
[36] D. Aguilera, A. Perez, R. Molina, S. Moreno, Appl. Catal., B 104 (2011) 144–150. https://doi.org/10.1016/j.apcatb.2011.02.019.
[37] J. Toniolo, A. Takimi, C. Bergmann, Mater. Res. Bull. 45 (2010) 672–676. https://doi.org/10.1016/j.materresbull.2010.03.001.
[38] Q. Tang, C. Wu, R. Qiao, Y. Chen, Y. Yang, Appl. Catal., A 403 (2011) 136–141. https://doi.org/10.1016/j.apcata.2011.06.023.
[39] F. Kovanda, K. Jirátová, Applied Clay Science, 53 (2011) 305–316. https://doi.org/10.1016/j.clay.2010.12.030.
[40] S. Kim, Y. Park, J. Nah, Powder Technology, 266 (2014) 292–298. https://doi.org/10.1016/j.powtec.2014.06.049.
[41] T. Xue, R. Li, W. Goa, Y. Goa, Q. Wang, A. Umar, J. Nanosci. Nanotechnol, 18 (2018) 3381–3386. https://doi.org/10.1166/jnn.2018.14627.
[42] H. Yang, J. Deng, Y. Liu, S. Xie, Z. Wu, H. Dai, Journal of Molecular Catalysis A: Chemical 414 (2016) 9–18. https://doi.org/10.1016/j.molcata.2015.12.010.
[43] L. Liu, Y. Song, Z. Fu, Q. Ye, S. Cheng, T. Kang, H. Dai, Appl. Surf. Sci. 396 (2017) 599–608. https://doi.org/10.1016/j.apsusc.2016.10.202.
[44] S. Carabineiro, X. Chen, M. Konsolakis, A. Psarras, P. Tavares, J. Órfão, M. Pereira, J. Figueiredo, Catalysis Today 244 (2015) 161–171. https://doi.org/10.1016/j.cattod.2014.06.018.
[45] G. Soylu, Z. Özçelik, I. Boz, Chem. Eng. J. 162 (2010) 380–387. https://doi.org/10.1016/j.cej.2010.05.020.

ALANNA SILVEIRA DE MORAES[1]

GABRIELA OLIVEIRA CASTRO PONCINELLI[1]

ARON SEIXAS TERRA RODRIGUES[1]

LAISE FAZOL DO COUTO[1]

SILVIA LUCIANA FÁVARO[2]

RITA DE CÁSSIA COLMAN [1]

[1]Universidade Federal Fluminense, Chemical Engineering and Petroleum Department, RJ, Brazil

[2]Universidade Estadual de Maringá – Mechanical Engineering Department, Maringá, PR, Brazil

NAUČNI RAD

PROUČAVANJE KATALITIČKE OKSIDACIJE TOLUENA KORIŠĆENJEM KATALIZATORA MEŠOVITIH OKSIDA Cu-Mn, Co-Mn I Ni-Mn

Uspešna sinteza AMn_2O_4 (A = Co, Cu, i Ni) spinela sagorevanjem rastvora postignuta je za manje vremena nego drugim metodama. Za oksidaciju toluena korišćeni su svi katalizatori sa istim odnosom gorivo/nitrat i istražen je odnos između njihovih svojstava i aktivnosti. Među njima, nikl manganit je pokazao najveću aktivnost, a promenom odnosa gorivo/nitrat se tražilo da se dobije najprikladnija struktura za proučavanu reakciju. Fizičkohemijska analiza je korišćena za definisanje karakteristika sintetizovanih katalizatora. Rezultati su pokazali uspešnu sintezu spinela i da u strukturi katalizatora postoje pikovi drugih materijala (pojedinačne oksidne faze). BET-BJH analize otkrile su mezoporozne strukture i, s obzirom na ograničenja opreme, sve su klasifikovane kao manje od 10 m^2/g. SEM slike dokazuju uticaj korišćenog sadržaja uree. Veličina čestica se povećava pri višim odnosima gorivo/nitrat. Uzorci NiMn1.67 i NiMn2.08 pokazali su veće i gušće, retko dispergovane klastere. Istovremeno, s obzirom na analizu reaktora i rezultate isptraživanja, utvrđeno je da sintetizovani katalizator sa odnosom gorivo/nitrat od 0,5 ima najbolje performanse u pogledu oksidacije toluena.

Ključne reči: sinteza sagorevanjem rastvora, odnos goriva i nitrata, manganit spineli, oksidacija toluena.